*This is the Author Accepted Manuscript (postprint) of:*
*Tacchini et al., 2012, NANO: Brief Reports and Reviews*
*Vol. 7, No. 3 (2012) 1250020 (10 pages)*
*https://doi.org/10.1142/S1793292012500208*

# SWCNTs as Electron Withdrawers in Nanocrystalline Anatase Photocatalysts

Ignacio Tacchini*, Eva Terrado, Alejandro Ansón-Casaos, M. Teresa Martínez

*Corresponding author: Ignacio Tacchini (itac@icb.csic.es)

Instituto de Carboquímica (ICB-CSIC), Zaragoza, Spain

Facultad de Ciencias de la Salud, Universidad San Jorge, Zaragoza, Spain

## Abstract

Single-walled carbon nanotube (SWCNT)/anatase TiO2 composite materials were prepared by successive solgel and hydrothermal processes. The composites contained thin SWCNT bundles embedded in aggregates of 12 nm anatase crystallites. A series of SWCNT/TiO2 photocatalysts was prepared with various SWCNT contents; a SWCNT content of 8 wt.% was found to be optimal for methylene blue (MB) degradation under combined UV/visible radiation. The optimized SWCNT/TiO2 composite demonstrated substantially higher photocatalytic activity than pure nanocrystalline anatase (5.2 times) and Degussa P-25 TiO2 powder (2.7 times). The MB degradation and mineralization processes were separately evaluated, and complete decomposition of MB was shown to take place. The presence of SWCNTs caused an increase in the visible light absorbance of TiO2; however, SWCNT/TiO2 composites did not show any photocatalytic ac- tivity when the UV part of the UV/visible light source was altered. Therefore, SWCNTs worked as acceptors for the TiO2 photoexcited electrons, but did not act as sensitizers for TiO2.

**Keywords:** Carbon nanotubes; titanium dioxide; photocatalysis; ultraviolet; visible light.

## 1. Introduction

The most active field of TiO2 photocatalysis is the degradation of organic compounds. [1] Many factors influence TiO2 photoactivity, such as specific surface area, pore size distribution, crystal size and the preparation method.[1] TiO2 has become an efficient photocatalyst in environmental decontamination for a large variety of organics, viruses, bacteria and algae, which can be degraded and mineralized to CO2, H2O and harmless inorganic anions. An important drawback for TiO2 utilization is that it is only photoactive under UV radiation and not under visible/infrared light. One of the strategies for improving the photoactivity of TiO2 materials is to synthesize them in the shape of small particles, rods and tubes with nanometric diameters,[2] reducing the migration path to the crystal surface (and consequently the possibility of the electron-hole pair recombination) while obtaining a larger catalytic surface. It is also known that TiO2-based composites usually demonstrate higher photoreactivities than pure TiO2 materials.[3] Carbon nanotube (CNT)/TiO2 composites have been fabricated by a range of different methods including mechanical mixing,[4] solgel synthesis,[5,6] electrospinning methods,[7,8] electrophoretic deposition[9] and chemical vapor deposition.[10] The morphological and physical properties of the composite materials depend on the preparation method. CNTs are usually treated with nitric/sulphuric acid before they are mixed with TiO2 or TiO2 precursors. Besides eliminating metal impurities, acid treatments create oxygen functional groups on CNTs that improve CNT dispersion in polar liquids and their compatibility with TiO2. As an alternative, dispersion of CNTs can be achieved in a surfactant. Gao et al.[6,11] prepared a series of CNT/TiO2 composites by a solgel method, starting from multiwalled carbon nanotube (MWCNT) dispersions in sodium dodecylbenzenesulphonate (SDBS) aqueous solutions. A composite material with 20 wt.% MWCNTs demonstrated a higher activity for the photodegradation of methylene blue (MB) than both pure TiO2 and MWCNT/TiO2 composites prepared without SDBS.

Two photoelectronic mechanisms have been proposed to explain the improved photocatalytic performance of CNT/TiO2 composites[12,13]: Either (i) CNTs withdraw the photoexcited electrons from TiO2, increasing the electron/hole pair lifetime and thus its reactivity, or (ii) CNTs act as TiO2 sensitizers, harvesting light photons and then inducing an electron/hole excited pair on TiO2. Yao et al.[14] prepared several CNT/TiO2

composites varying CNT type and TiO2 nanoparticle size in order to find an optimized interaction between the com- ponents. The authors concluded that CNTs acted as electron traps and reported that single-walled carbon nanotube (SWCNT) bundles bend and wrap more easily than MWCNTs around TiO2 nanoparticles, resulting in higher photocatalytic activities.[14] However, Yao et al.[14] did not comment on the possibility of TiO2 sensitization by CNTs, which is suggested by other literature reports.[12,13]

In the present work, nanocrystalline TiO2 was prepared by successive solgel/hydrothermal processes and mixed with SWCNTs that had been previously dispersed in a SDBS aqueous solution. A series of SWCNT/TiO2 hybrid materials was obtained varying the ratio between the components. The ability of the composite materials to destroy a model compound (MB) was evaluated under UV-visible light. A SWCNT/TiO2 composite with optimal SWCNT content demonstrated substantially higher photocatalytic activity than pure nanocrystalline anatase and Degussa P-25 TiO2. Despite the fact that remarkable activities were observed under UV-visible illumination, SWCNT/TiO2 composites were not active when UV light was altered. An interesting point here is to remark that the composites did not show any photocatalytic capability under visible irradiation in spite of their obvious visible light absorption (SWCNTs did not behave as sensitizers for TiO2). The apparent discrepancies between those findings and some literature reports will be discussed.

## 2. Experimental

### 2.1. SWCNT synthesis and dispersion

SWCNTs were synthesized by the arc-discharge method using graphite electrodes and Ni/Y catalyst (2/0.5 atomic %). This SWCNT material has been previously characterized.[15,16] About 100 mg of the as-grown SWCNTs were mixed with 50 mL of a 1% SDBS aqueous solution. The mixture was sonicated for 1 h using a UP 400S Hielsher tip (0.5 cycle, 60% amplitude) and spun for 30 min at 13 000 rpm (23 000 g) in a Hermle Z383 centrifuge. The super- natant was decanted and directly utilized for the preparation of SWCNT/TiO2 composites. As-prepared supernatants are very stable suspensions of well-dispersed SWCNTs. The purity of the SWCNT dispersion was evaluated by near infrared spectroscopy following a procedure similar to that reported by Itkis et al.[17] The purity ratio of the SWCNT dispersion was 0.078.

### 2.2. Preparation and characterization of SWCNT/TiO2 composites

Nanocrystalline TiO2 and SWCNT/TiO2 composite materials were prepared by a combination of solgel and hydrothermal methods. In a typical experiment, 5 mL of titanium isopropoxide was diluted in 50 mL of isopropanol. The solution was added dropwise into a mixture containing isopropanol (26 mL), water and the SWCNT aqueous dispersion. Nanocrystal- line TiO2 and five different SWCNT/TiO2 composites (labeled as 1, 2, 3, 4 and 5) were prepared with increasing SWCNT contents (SWCNTaq-Ti isopropoxide volume ratios of 2.6, 5.2, 10.4, 20.8, 41.6). The resulting powders were aged overnight in the reaction mixture, filtered, washed and dried at 105C. The materials were subsequently mixed with 20 mL of a 1:1 isopropanol/water solution and were treated at 200C for 24 h in a 25-mL autoclave. The materials were filtered, rinsed with distilled water and dried at 105C. The described SWCNT/TiO2 synthesis procedure takes advantage of two experimental facts: (a) SWCNT are puri¯ed and disaggregated through centrifugation in SDBS solutions[18,19] and (b) the presence of SDBS increases the compatibility of SWCNT with TiO2.[6,11] The materials were characterized by X-ray diffraction (XRD, Bruker D8 Advance Series 2 diffractometer), scanning electron microscopy (SEM, Hitachi S-3400N), transmission electron microscopy (TEM, JEOL-200FXII), nitrogen adsorption at 196C (Micromeritics ASAP 2020), UV-visible spectroscopy (Shimadzu UV-3600 equipped with an integrating sphere accessory), elemental analysis (Carlo Erba 1108), Raman spectroscopy (Jovin Yvon HR-8400UV) and photoluminescence spectroscopy (HORIBA JOBIN YVON Fluoromax D).

### 2.3. Photocatalytic activity measurements

Photocatalytic activity measurements were carried out in a photocatalytic reactor consisting of a 1-litre quartz vessel (diameter 1⁄4 12 cm) with two valves (air entrance and purge), a sample collector and two 8W Daylight lamps (Hitachi). The reactor configuration and the emission spectrum corresponding to the lamps are shown in Fig. 1. The lamps are cylindrical (3 X15 cm) and the separation between their centers is 7 cm. STEM filters were utilized to cover the Daylight lamps, eliminating UV radiation ( < 400 nm) in test experiments with only visible light. According to specifications from the provider, the 413T10 film is transparent to visible light, while most of UV light is captured. For the photocatalysis experiments, 300 ml of 5 ppm MB aqueous solution was

introduced into the reactor with 300 mg of the tested photocatalyst (the SWCNT/TiO2 composites, the nanocrystalline TiO2 or the commercial Degussa P-25 TiO2Þ. The mixture was stirred in darkness at 250 rpm for 2 h to assure catalyst surface saturation with the MB. The mixtures were subsequently aerated and illuminated by the lamps. The 3-mL samples were regularly extracted and filtered. The MB degradation was monitored on a UV-visible Spectrometer (Shi- madzu UV-3600) at 662 nm. MB degradation occurred neither under UV-visible radiation without TiO2, nor in the presence of TiO2 without UV-visible radiation. In order to confirm that the loss of color observed during the photocatalysis experiments was due to the complete mineralization of MB, the purge gas from the photoreactor was blown through a H2O adsorbent (Mg(ClO4)2 and a CO2 adsorbent (NaOH on an inert support) consecutively. The powders resulting from the CO2 adsorption (containing the adsorbent material and the adsorbed CO2 were characterized using Carlo-Erba 1108 elemental analysis equipment. The MB mineralization for each photocatalyst material was calculated from the carbon content in the CO2 trap after 2 h of operation. A control experiment without the photocatalyst was performed to account for the small CO2 amounts due to other sources different from MB decomposition, including CO2 impurities in the purge gas and in the CO2 adsorber.

## 3. Results and Discussion

### 3.1. Characterization

XRD analysis demonstrated that amorphous titanium dioxide resulting from the solgel process was converted into anatase phase TiO2 during the autoclave treatment at 200C. XRD patterns of the SWCNT/TiO2 composite materials are shown in Fig. 2. For all the samples, the difractogram contained Bragg's reflections at about 25; 38; 48; 54, and 63 corresponding to the (101); (004); (200); (211) and (204) tetragonal crystal planes of anatase TiO2. Anatase crystallite sizes were calculated using the Scherrer formula. The average crystallite size (Table 1) obtained from XRD data was around 11 nm. Raman spectra of the hydrothermally treated SWCNT/TiO2 composites are shown in Fig. 3. Spectral features of both anatase TiO2 and SWCNTs can be observed. Anatase bands in the composites are broader than in commercial anatase owing to their smaller particle and crystallite size.[20,22] The relative Raman intensity of the SWCNT G-band at around 1600 cm-1 increased with the SWCNT content.

SEM images (Fig. 4) showed a composite material where the presence of both nanocrystalline TiO2 and SWCNTs can be identified. TEM images (Fig. 5) revealed the presence of TiO2 crystallites of 911 nm, in good agreement with sizes calculated from XRD analysis. The SWCNT/TiO2 composites can be described as random mixtures of aggregated TiO2 crystallites and SWCNT thin bundles. Specific surface area of the different SWCNT/TiO2 composites ranged between 100 and 125 m2/g (listed in Table 1). Such values are higher than surface areas of pure nanocrystalline TiO2 and Degussa P-25. Specific surface areas of SWCNT/TiO2 composites are between those of pure nanocrystalline TiO2 and titanate nanotubes synthesized by the hydrothermal method, which typically exhibit 300 m2/g.2

Elemental analysis indicated that the carbon content in the SWCNT/TiO2 composite samples was in the range of 110% (listed in Table 1). High carbon contents correspond to composites with high SWCNT charge. Carbon determined by elemental analysis could come from SWCNTs or from residual SDBS molecules remaining in the final product. However, the absence of sulfur in the elemental analysis indicated the removal of the surfactant during the washing steps. Thus, the determined carbon content was due only to the SWCNT fraction.

Despite the small amounts of SWCNTs in the SWCNT/TiO2 composite samples, relevant changes were detected in their optical properties. Visible light absorption intensity was substantially increased by the presence of SWCNTs (Fig. 6). The optical absorption edge of the composites showed an appreciable shift to the visible light region, which increased with the SWCNT content. This effect has been previously described in MWCNT/TiO2 composites,[23] and is caused by visible light absorption on the carbon phase. The presence of the carbon material gives the CNT/TiO2 composites their gray/black color. However, we did not observe the sensitization of TiO2 by the CNTs in the photo- catalytic experiments, as will be discussed below.

Photoluminescence (PL) emission spectra are useful to explore the efficiency of charge carrier transfer in semiconductor nanoparticles, since the PL emission is a consequence of the recombination of the electron-hole pairs.[24] The PL emission spectra of the samples were examined in the range of 2.93.5 eV and are shown in Fig. 7. The spectrum of the nanocrystalline TiO2 revealed a prominent peak at 3.26 eV (381.5 nm), which

corresponds to the anatase band gap. This energy value is in agreement with the results previously reported in the literature.[24,25] The spectra of the SWCNT/TiO2 composites showed intensities decreasing with increasing SWCNT contents. The PL results are in good agreement with those reported by Yao et al.[14] for SWCNT composites containing 100-nm TiO2 particles.

Assuming that the PL emission is mainly originated by the recombination of excited electrons and holes, a lower PL intensity could be due to a lower recombination rate of those electrons and holes under light irradiation.[10,26] The electrons promoted from the valence band to the conduction band could migrate from the TiO2 to the acceptor SWCNTs through the solidsolid interphase, leading to the decrease in the recombination rate. However, it has been recently pointed that PL analysis in terms of PL intensity should not be considered as a direct measurement of the recombination rate due to the quenching of the emitted PL signals by the CNTs.[27]

**3.2. Photocatalytic activity**

Like other similar dyes, MB is commonly utilized as a model compound in photocatalysis since it can be found in water effluents from textile industries. In the present article, the photocatalytic activity of SWCNT/TiO2 composites was tested for MB degradation and was compared with those of a pure TiO2 material (nanocrystalline TiO2Þ and commercial TiO2 (Degussa P-25). Figure 8 shows control experiments in darkness for the MB physical adsorption on various photocatalysts. Most of the MB adsorption took place within the first 10 min of contact in the stirred dispersion and MB concentration was nearly constant after 30 min in all the cases. The total amount of adsorbed MB followed the same trend as the specific surface area (Table 1). It can be concluded that MB adsorption occurred well before 2 h, which was the waiting time previous to degradation experiments under UV-visible illumination.

Figure 9 shows the change in concentration when MB aqueous solutions were illuminated with UV-visible radiation in the presence of the studied photocatalysts. The reaction followed apparent first- order kinetics that is in agreement with the generally observed Langmuir-Hinshelwood kinetics model:

$$r = dC / dt = k\theta = kKc / ( 1+KC' )$$

where r is the reaction rate, C is the MB concentration at time t, is the surface coverage, k is the rate constant and K is the Langmuir constant. This equation can be simplified to an apparent first-order equation:

ln (C/C0) = kKt = kappC

where C0 is the MB concentration when UV-visible illumination is switched on. The apparent first-order rate constants, kapp1⁄2min1 and the percentages of photodegraded MB obtained with the different tested photocatalysts after 2 h are listed in Table 1.

The photocatalytic efficiency of the SWCNT/ TiO2 composite samples was significantly higher than that of pure nanocrystalline TiO2. MB degradation with SWCNT/TiO2 (3), (4) and (5) was much more efficient than with SWCNT/TiO2 (1) and (2) samples, suggesting that a minimum SWCNT content of 4.5 wt.% was required for significant enhancement of the nanocrystalline TiO2 photo- catalytic activity. The efficiency of the SWCNT/ TiO2 (4) sample was substantially higher than that of Degussa P-25, reaching degradation levels of 85% in 2 h. The MB decomposition rate constant (kapp for the SWCNT/TiO2 (4) photocatalyst was 5.2 times that for nanocrystalline TiO2 and 2.7 times that for P-25 TiO2. The enhancement factor with respect to P-25 was similar to that reported by Yao et al.[14] for phenol degradation with composites of 100-nm TiO2 particles containing 4.7 wt.% SWCNTs. However, while Yao et al.[14] did not find substantial changes with the SWCNT content, we found that the optimal SWCNT loading in the composites was 8 wt.%. Higher loadings produced a decrease in the TiO2 photocatalytic activity, which could be associated to a decrease in the light capture efficiency In fact, the SWCNT content in the SWCNT/TiO2 (5) sample resulted to be above the optimal value. The SWCNT/TiO2 (5) material showed the greatest decrease in the PL intensity among the studied samples (Fig. 7), while its photocatalytic efficiency was lower than for SWCNT/TiO2 (4). The decrease in the light capture efficiency for SWCNT/TiO2 (5) could be due to the light screening produced by the increasing carbon phase content.

Although MB photodegradation was studied by UV-visible colorimetric measurements, the amount of CO2 evolving from the photoreactor was also analyzed. The results are listed in Table 1, where the percentage of mineralization can be compared with colorimetric degradation. A mineralization level of 81% was obtained after 2 h with the SWCNT/ TiO2 (4), compared with the 51% reached by the Degussa P-25 TiO2 under the

same experimental conditions. It can be concluded that color losses observed during photocatalysis experiments were mostly due to the complete decomposition of MB instead of other processes such as the photoreduction of MB to leuco-methylene blue (which is color- less) or the partial degradation of MB to aromatic intermediates. Four main causes have been proposed to explain the positive influence of SWCNTs on the TiO2 photocatalytic activity[12,13]: TiO2 band gap narrowing, TiO2 sensitization, increase in the surface area and reduction in the electron-hole recombination rate. Ideally, an increase in the surface area is always an advantage in catalysis since large areas favor the contact between the catalyst and reactant molecules. In order to investigate the other possible effects, the series of MB photocatalysis experiments were repeated with the Daylight lamps covered by a STEM 413T10 filter, which cut off radiation of wavelengths under 400 nm. It was observed that the MB underwent no substantial degradation with any of the tested photocatalysts under visible radiation (without the UV light component). Ideally, both TiO2 band gap narrowing and TiO2 sensitization should produce some photoactivity under visible light. Therefore, our results would suggest that the improved photoactivity of SWCNT/TiO2 composites was mainly caused by a reduction in the electron-hole recombination rate. This fact could be directly related to the electron acceptor character of SWCNTs.

The results presented here apparently disagree with some literature reports that claim visible light photocatalytic activity for CNT/TiO2 composites.[23,29,31] We suggest that such apparent discrepancy could be explained by differences existing between the composite preparation in those reports and the protocol utilized in the present work. In the cases when visible light photocatalytic activity was detected[23,29,30] a high temperature treatment above 400C was performed after mixing CNTs with TiO2 or the TiO2 precursor. However, we did not utilize the high temperature treatment because phase transformation of amorphous titanium oxide into anatase TiO2 was elected through a hydrothermal treatment at 200C. It is known that high temperature treatments of TiO2 or TiO2 precursors in the presence of an organic carbon source lead to carbon-doped TiO2 that demonstrate visible light photocatalytic activity.[32,34] We suggest that CNTs or carbonaceous impurities of the CNT samples could act as carbon doping sources for TiO2 during the treatments at temperatures higher than 400C. This could produce visible

light photoactivity, but such effect would not be due to the intrinsic electrophotonic properties of CNTs.

Another possibility has been recently reported by Vijayan et al.[31] The authors prepared composite photocatalysts containing nitric acid-treated SWCNTs and titanium oxide nanotubes. A low temperature treatment was developed for composite preparation; however, the authors found that TiOC bonds were formed between the titania nanotubes and the SWCNTs during the hydration dehydration preparation cycle. In the present work, we did not apply any acid treatment which could have chemically functionalized SWCNTs and thus no TiOC interactions were formed. Our results indicate that CNTs do not sensitize TiO2 if they are not allowed to chemically react with TiO2; however, SWCNTs always behave as electron withdrawers, increasing the electron-hole pair life-time and thus the TiO2 photocatalytic activity.

**4. Summary**

SWCNT/TiO2 composites were prepared by a combined solgel/hydrothermal method and were utilized as the photocatalysts for the removal of an organic dye (MB) from water. Nanocrystalline anatase TiO2 was synthesized in a liquid medium containing a surfactant and well-dispersed SWCNTs. A SWCNT content of 8 wt.% in the SWCNT/TiO2 composites was optimal for producing maximum enhancement in the photocatalytic activity towards MB degradation and mineralization. The photoactivity of such a composite photocatalyst, measured as the apparent kinetic constant, was 5.2 times that of nanocrystalline TiO2 and 2.7 times that of commercial Degussa P-25. Photoexcited electrons from nanocrystalline TiO2 anatase could be withdrawn by SWCNTs, causing a lengthening of the electron-hole pair lifetime and thus, in the photocatalytic activity.

SWCNT loadings above the optimum content in the composite would produce a substantial decrease in the light density reaching the TiO2 particles. SWCNT/TiO2 composites absorb visible light because of the presence of SWCNTs. However, SWCNT/TiO2 composites did not show photo- activity under visible light, indicating that SWCNTs did not behave as sensitizers for TiO2.

**Acknowledgments**

This work was funded by the Government of Ara- gon and \La Caixa" Ref. GA-LC-041/2008 and by the Spanish Ministry of Science and Innovation Ref. EUI2008-00152.

**References**

1. O. Carp, C. L. Huisman and A. Reller, Prog. Solid. State. Ch. 32, 33 (2004).

2. I. Tacchini, E. Terrado, A. Ansón and M. T. Mar- tínez, J. Mater. Sci. 46, 2097 (2011).

3. G. Li and K. A. Gray, Chem. Phys. 339, 173 (2007).

4. B. Ahmmad, Y. Kusumoto, S. Somekawa and M. Ikeda, Catal. Commun. 9, 1410 (2008).

5. W. Wang, P. Serp, P. Kalck and J. L. Faria, Appl. Catal. B-Environ. 56, 305 (2005).

6. K. S. Lin, C. C. Lo and N. B. Chang, NANO 3, 257 (2008).

7. G. Hu, X. Meng, X. Feng, Y. Ding, S. Zhang and M. Yang, J. Mater. Sci. 42, 7162 (2007).

8. S. Aryal, C. K. Kim, K. W. Kim, M. S. Khil and H. Y. Kim, Mater. Sci. Eng. C 28, 75 (2008).

9. J. Cho, S. Schaab, J. A. Roether and A. R. Boc- caccini, J. Nanopart. Res. 10, 99 (2008).

10. H. Yu, X. Quan, S. Chen and H. Zhao, J. Phys. Chem. C 111, 12987 (2007).

11. B. Gao, G. Z. Chen and G. L. Puma, Appl. Catal. B-Environ. 89, 503 (2009).

12. K. Woan, G. Pyrgiotakis and W. Sigmund, Adv. Mater. 21, 2233 (2009).

13. R. Leary and A. Westwood, Carbon 49, 741 (2011).

14. Y. Yao, G. Li, S. Ciston, R. M. Lueptow and K. A. Gray, Environ. Sci. Technol. 42, 4952 (2008).

15. A. Anson, J. Jagiello, J. B. Parra, M. L. Sanjuan, A. M. Benito, W. K. Maser and M. T. Martinez, J. Phys. Chem. B 108, 15820 (2004).

16. F. Pico, J. M. Rojo, M. L. Sanjuan, A. Anson, A. M. Benito, M. A. Callejas, W. K. Maser and M. T. Martinez, J. Electrochem. Soc. 151, A831 (2004).

17. M. E. Itkis, D. E. Perea, S. Niyogi, S. M. Rickard, M. A. Hamon, B. Zhao and R. C. Haddon, Nano Lett. 3, 309 (2003).

18. A. Ansón-Casaos, J. M. Gonzalez-Domínguez and M. T. Martínez, Carbon 48, 2917 (2010).

19. H. Cathcart and J. N. Coleman, Chem. Phys. Lett. 474, 122 (2009).

20. A. J. Maira, K. L. Yeung, C. Y. Lee, P. L. Yue and C. K. Chan, J. Catal. 192, 185 (2000).
21. A. Orendorz et al., Surf. Sci. 601, 4390 (2007).
22. S. Santangelo, G. Messina, G. Faggio, A. Donato, L. De Luca, N. Donato, A. Bonavita and G. Neri, J. Solid State Chem. 183, 2451 (2010).
23. W. Wang, P. Serp, P. Kalck and J. L. Faria, J. Mol. Catal. A-Chem. 235, 194 (2005).
24. F. B. Li and X. Z. Li, Chemosphere 48, 1103 (2002).
25. H. Tang, H. Berger, P. Schmid and F. Levy, Solid State Commun. 92, 267 (1994).
26. J. G. Yu, L. Yue, S. W. Liu, B. B. Huang and X. Y. Zhang, J. Coll. Interf. Sci. 90, 595 (2009).
27. J. Yu, T. Ma and S. Liu, Phys. Chem. Chem. Phys. 13, 3491 (2011).
28. Y. J. Xu, Y. B. Zhuang and X. Z. Fu, J. Phys. Chem. C 114, 2669 (2010).
29. W. Chen, Z. Fan, B. Zhang, G. Ma, K. Takanabe, X. Zhang and Z. Lai, J. Am. Chem. Soc. 133, 14896 (2011).
30. K. Zhang, F. J. Zhang, M. L. Chen and W. C. Oh, Ultrason. Sonochem. 18, 765 (2011).
31. B. K. Vijayan, N. M. Dimitrijevic, D. Finkelstein- Shapiro, J. Wu and K. A. Gray, ACS Catal. 2, 223 (2012).
32. Z. Wu, F. Dong, W. Zhao, H. Wang, Y. Liu and B. Guan, Nanotechnology 20, 235701 (2009).
33. F. Dong, H. Wang and Z. Wu, J. Phys. Chem. C 113, 16717 (2009).
34. X. Lin, F. Rong, X. Ji and D. Fu, Micropor. Meso- por. Mater. 142, 276 (2011). 1250020-10 July 27, 2012

**Figures**

**Fig. 1.** Schematic configuration of the photoreactor used to carry out MB photodegradation and the emission spectrum of Daylight lamps (Hitachi).

**Fig. 2.** XRD patterns for: (a) Nanocrystalline TiO2, (b) SWCNT/TiO2 (5), (c) SWCNT/TiO2 (4), (d) SWCNT/TiO2 (3), (e) SWCNT/TiO2 (2) and (f) SWCNT/TiO2 (1).

**Fig. 3**. Raman spectra (laser at 532 nm) for: (a) Nanocrystalline TiO2, (b) SWCNT/TiO2 (5), (c) SWCNT/TiO2 (4), (d) SWCNT/ TiO2 (3), (e) SWCNT/TiO2 (2), and (f) SWCNT/TiO2 (1).

**Fig. 4.** Scanning electron microscopy image of the SWCNT/ TiO2 (4) composite sample showing a material consisting of SWCNT bundles interwoven with nanocrystalline TiO2 aggregates.

**Fig. 5.** Transmission electron microscopy images of a SWCNT/TiO2 composite sample showing: (a) TiO2 crystallites of 911 nm and (b) a SWCNT bundle surrounded by aggregated TiO2 particles.

**Fig. 6.** UV-visible spectra for: (a) SWCNT/TiO2 (5), (b) SWCNT/TiO2 (4), (c) SWCNT/TiO2 (3), (d) SWCNT/TiO2 (2), (e) SWCNT/TiO2 (1), (f) P-25, and (g) nanocrystalline TiO2.

**Fig. 7.** The PL spectra for: (a) SWCNT/TiO2 (5), (b) SWCNT/TiO2 (4), (c) SWCNT/TiO2 (3), (d) SWCNT/ TiO2 (2), (e) SWCNT/TiO2 (1), and (f) nanocrystalline TiO2.

**Fig. 8.** Rates of MB adsorption (in darkness) on (a) P-25, (b) SWCNT/TiO2 (1), (c) SWCNT/TiO2 (2), (d) SWCNT/TiO2 (3), (e) SWCNT/TiO2 (4), and (f) SWCNT/TiO2 (5) (Initial concentration Ci =5 ppm).

**Fig. 9.** Rates of photocatalyzed degradation of the MB under UV-visible irradiation in the presence of (a) nanocrystalline TiO2, (b) SWCNT/TiO2 (1), (c) SWCNT/TiO2 (2), (d) Degussa P-25, (e) SWCNT/TiO2 (3), (f) SWCNT/TiO2 (5), and (g) SWCNT/TiO2 (4).

**Tables**

**Table 1.** Elemental carbon content (wt.% C), specific surface area (SBETÞ, X-ray diffraction crystallite size and photocatalytic activity.

Figure 1

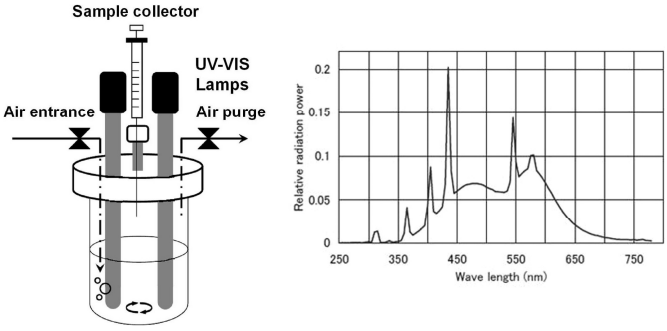


Figure 2

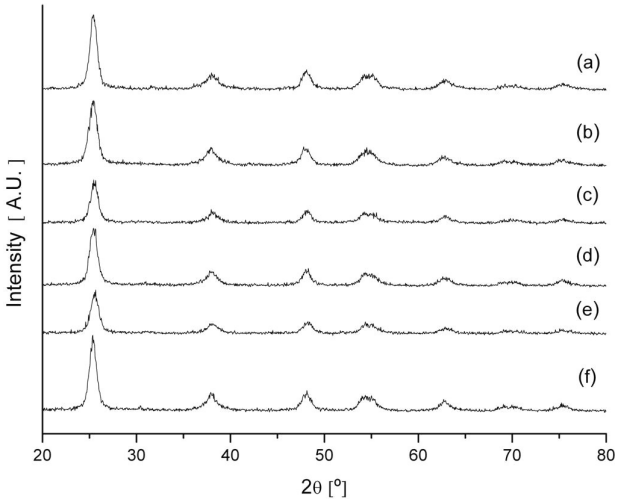


Figure 3

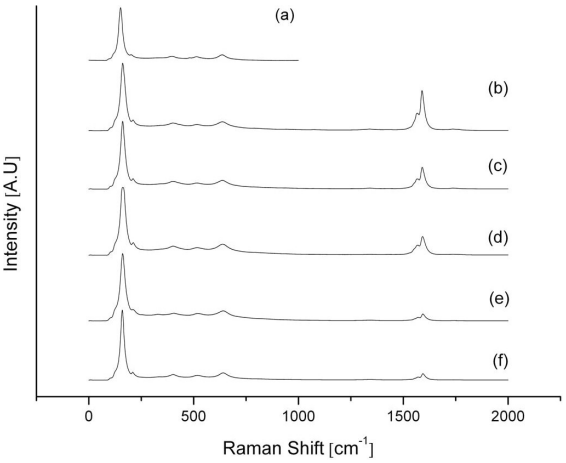

Figure 4

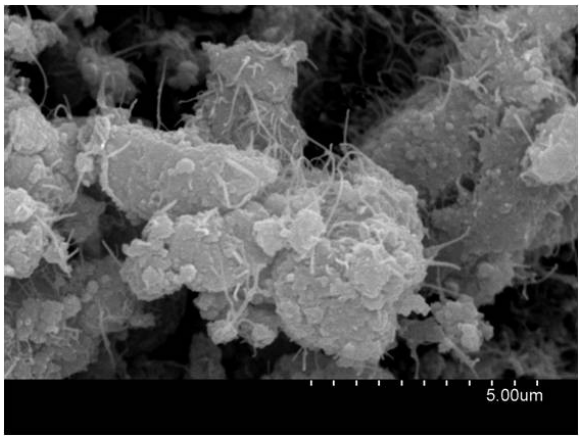


Figure 5

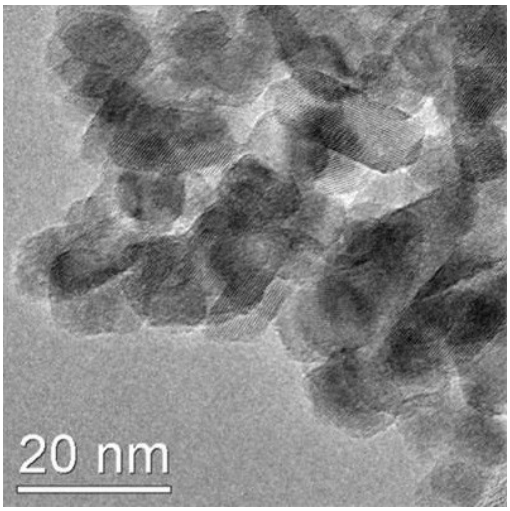


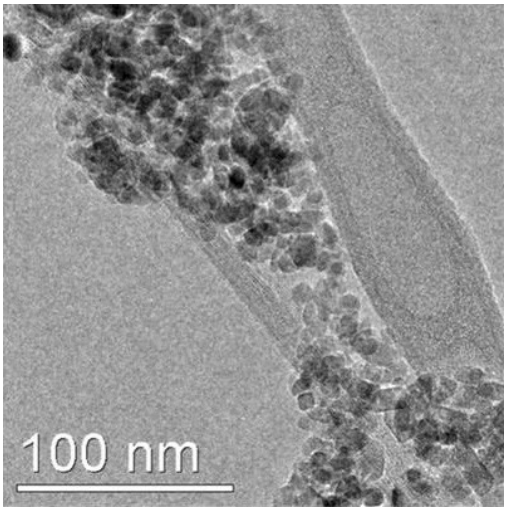

Figure 6

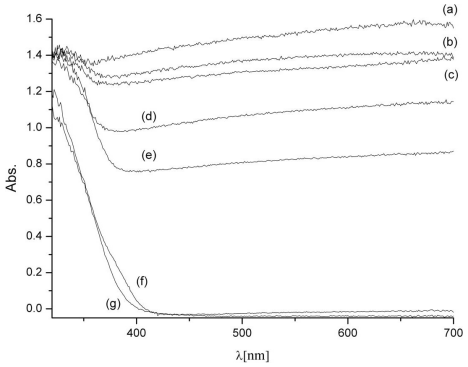


Figure 7

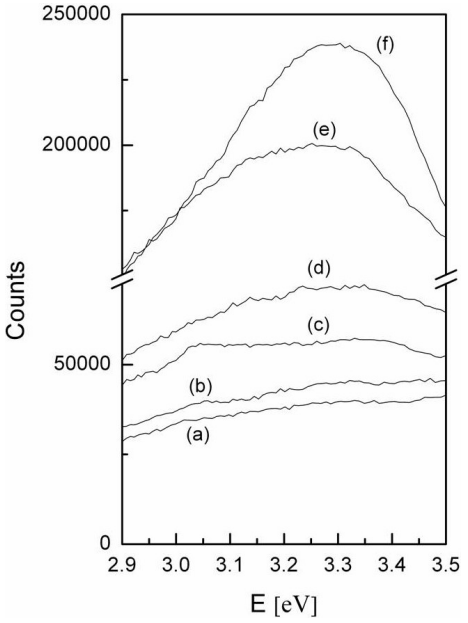


Figure 8

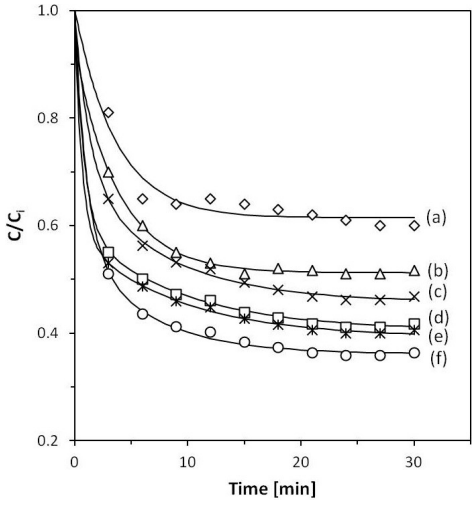

Figure 9

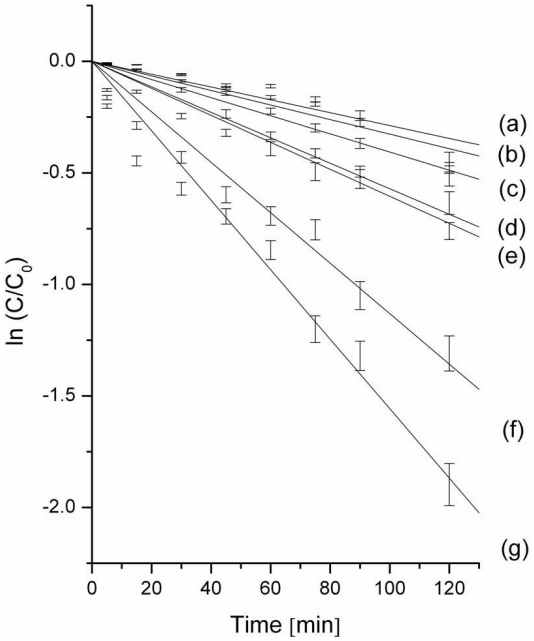


Table 1

| Sample | C [wt.%] | $S_{BET}$ [$m^2/g$] | $\chi_c$ [nm] | $k_{app} \cdot 10^3$[$min^{-1}$] | Degradation [%][b] | Mineralization [%][b] |
|---|---|---|---|---|---|---|
| P-25 | 0 | 50 | 32A/52R[a] | 5.7 | 51 | 37 |
| Nanocrystalline $TiO_2$ | 0 | 70.4 | 13 | 3 | 10 | 4 |
| SWCNT/$TiO_2$ (1) | 1.3 | 116 | 12 | 3.3 | 15 | 9 |
| SWCNT/$TiO_2$ (2) | 2.5 | 128 | 12 | 4.1 | 28 | 23 |
| SWCNT/$TiO_2$ (3) | 4.5 | 144 | 11 | 6.1 | 53 | 47 |
| SWCNT/$TiO_2$ (4) | 8.3 | 148 | 11 | 15.6 | 85 | 81 |
| SWCNT/$TiO_2$ (5) | 11.8 | 165 | 12 | 11.3 | 73 | 67 |

[a]Degussa P-25 is a 2/1 mixture of anatase/rutile phases; crystallite sizes are given for both phases respectively.
[b]Percentage of MB that was degraded and mineralized after 2 h operation.